



# An observation-based climatology of middle atmospheric meridional circulation

Thomas von Clarmann<sup>1</sup>, Udo Grabowski<sup>1</sup>, Gabriele P. Stiller<sup>1</sup>, Beatriz M. Monge-Sanz<sup>2</sup>,  
Norbert Glatthor<sup>1</sup>, and Sylvia Kellmann<sup>1</sup>

<sup>1</sup>Karlsruhe Institute of Technology, Institute of Meteorology and Climate Research,  
Karlsruhe, Germany

<sup>2</sup>University of Reading, Department of Meteorology, Reading, UK

**Correspondence:** T. von Clarmann (thomas.clarmann@kit.edu)

**Abstract.** Measurements of long-lived trace gases (SF<sub>6</sub>, CFC-11, CFC-12, HCFC-12, CCl<sub>4</sub>, N<sub>2</sub>O, CH<sub>4</sub>, H<sub>2</sub>O, and CO) performed with the Michelson Interferometer for Passive Atmospheric Sounding (MIPAS) have been used to infer the stratospheric and mesospheric meridional circulation. The MIPAS data set covers the time period from July 2002 to April 2012. The method used for this purpose was the direct inversion of the two-dimensional continuity equation. Monthly climatologies of circulation fields are presented along with their variabilities. Stratospheric circulation is found to be highly variable over the year, with a quite robust annual cycle. The new method allows to track the evolution of various circulation patterns over the year in more detail than before. The deep branch of the Brewer-Dobson circulation and the mesospheric overturning pole-to-pole circulation are not separate but intertwined phenomena. The latitude of stratospheric uplift in the middle and upper stratosphere is found to be quite variable and is not always found at equatorial latitudes. The usual schematic of stratospheric circulation with the deep and the shallow branch of the Brewer-Dobson circulation and the mesospheric overturning circulation is an idealization which best describes the observed atmosphere around Equinox. Sudden stratospheric warmings cause increased year-to year variability.

## 1 Introduction

The Brewer-Dobson circulation (BDC, Brewer and Dobson 1949; Dobson 1956), with its lower and upper branch as well as the mesospheric overturning circulation, is the major transport pattern in the stratosphere. As such it governs the distribution of atmospheric constituents in the stratosphere. The BDC therefore controls the distribution of radiative gases, such as ozone and water vapour, as well as aerosols, affecting major chemistry-climate processes (Dunkerton, 1978; Plumb, 2002).

Possible changes in the intensity of the BDC as a consequence of climate change have been proposed by, e.g., Butchart et al. (2006) and triggered observation-based studies by Engel et al. (2009), using balloon-borne observations, and Stiller et al. (2012b), as well as Haenel et al. (2015), using satellite data. These studies based on satellite data suggest that the true picture of middle atmospheric circulation is far more detailed and far too complicated to be characterized merely by a scalar intensity of the circulation. Also offline model simulations driven by ERA-Interim analysis data confirmed this heterogeneous picture for



the stratosphere (Diallo et al., 2012; Monge-Sanz et al., 2012; Ploeger et al., 2015b). A shift of the entire circulation pattern by 5° to the South below 800 K and a widening of the tropical pipe above that altitude have been detected by Stiller et al. (2017).  
25 The relative importance of transport versus mixing has been investigated by, e.g., Garny et al. (2014) or Ploeger et al. (2015a). Structural changes of the BDC and evidence of a transition branch situated below the shallow branch have been reported by Lin and Fu (2013) and Diallo et al. (2019).

The polar winter downward branch of the mesospheric overturning circulation which brings large amounts of mesospheric NO<sub>x</sub>-rich air down into the stratosphere where it participates in ozone chemistry has been analyzed in depth by, e.g., Funke et al. (2005). It could be shown that the NO<sub>x</sub> flux into the stratosphere depends both on the thermospheric source strength which depends largely on solar particle precipitation and the strength of subsidence of air into the stratosphere in the polar winter vortex (Funke et al., 2008, 2011, 2014b, a, 2017). In this context, major stratospheric warmings play an essential role and are coupled with the lower atmosphere (Funke et al., 2010). Perturbations of stratospheric composition by downward transport of air into the middle atmosphere have also been investigated by Smith et al. (2011).  
30

In this study we aim to provide a more detailed picture of the meridional middle atmospheric circulation better resolved in space and time. For this purpose, we infer circulation vectors from measurements of long-lived trace gases from July 2002 to April 2012 obtained with the Michelson Interferometer for Passive Atmospheric Sounding (MIPAS, Fischer et al. 2008). From these we calculate a climatology<sup>1</sup> of the circulation in terms of multi-annual monthly means along with their variability over the years.  
35

First we present the methods and data sets used for our analysis (Section 2). This includes a description of the method of the direct inversion of the continuity equation (Section 2.1), of the trace gas data sets used (Section 2.2), and our scheme to calculate climatologies from the monthly circulation patterns (Section 2.3). Our derived climatologies of middle atmospheric circulation are discussed along with related variabilities in Section 3. Finally, in Section 4, we summarize our results, draw conclusions on their plausibility, and identify possible future work.  
40

## 45 2 Method and Data

Stratospheric circulation is inferred from monthly zonal mean mixing ratio distributions of long-lived tracers by the direct inversion of the continuity equation, using the method by von Clarmann and Grabowski (2016). Zonal mean volume mixing ratio fields are calculated from global trace gas distributions retrieved from limb emission spectra measured with MIPAS. Resulting circulation fields are analyzed in terms of first and second moment statistics to provide a climatology of the middle atmospheric circulation.  
50

---

<sup>1</sup>Conceding that ten years is often not considered as a climatologically relevant period of time, we still call these multi-year monthly mean circulation patterns ‘climatologies’, mainly in order to distinguish them from ‘monthly means’ which commonly are understood to refer to a specific year, as compiled, e.g., by the SPARC Data Initiative by Hegglin and Tegtmeier (2011); Hegglin et al. (2013); Hegglin and Tegtmeier (2017) or Tegtmeier et al. (2013, 2016). Doing this, we use the term ‘climatology’ in its widest sense.



## 2.1 The Direct Inversion of the Continuity Equation

The direct inversion of the continuity equation uses the scheme developed by von Clarmann and Grabowski (2016). This approach avoids certain limitations associated with the traditional observation-based characterization of the circulation via the mean age of stratospheric air. These are: (a) no age spectra (Andrews et al., 1999; Waugh and Hall, 2002) are required; 55 (b) the so-called ‘over-aging’ due to subsidence of mesospheric air depleted in tracer concentrations (Stiller et al., 2012b; Reddmann et al., 2001; Ray et al., 2017) does not bias the analysis because observation-based upper boundary mixing ratios of these gases are used, and (c) we provide circulation fields resolved in space and time. By doing so we can trace back the causes of possible discrepancies between model data and observation-based data better than with the age-based method. The observational information provided by the age-of-air method is only available as the integrated travel time of the air parcel 60 since it entered the stratosphere.

In the next subsection we shortly summarize the basic rationale behind this approach. Thereafter, updates of the related software (Analysis of Stratospheric Circulation Using Spectroscopic Measurements, ANCISTRUS) are described.

### 2.1.1 The General Approach

The prognostic formulation of the continuity equation allows to predict later trace gas and air density distributions when their 65 initial values as well as the velocities, mixing coefficients and source/sink terms are known. We invert this equation to obtain velocities and (optionally) mixing coefficients from given air density and trace gas distributions at different times. For this purpose, first the prediction step is formalized, using a matrix which contains the partial derivatives of the later atmospheric state with respect to the initial atmospheric state. From this we calculate the Jacobian containing the partial derivatives of the final atmospheric state with respect to the velocities and mixing coefficients. A constrained inversion of the prognostic equation 70 involving the latter Jacobian finally gives the field of velocities and mixing coefficients. Since, due to correlation of velocities and atmospheric composition, inferred velocities are not the zonally averaged velocities but include eddy transport effects, we call the inferred velocities ‘effective velocities’. For further details, see von Clarmann and Grabowski (2016), and Appendix A.

### 2.1.2 Recent Updates and Current Setup

75 The major amendment to the code since von Clarmann and Grabowski (2016) has been the inclusion of sinks of CCl<sub>4</sub>, CFC-11, CFC-12, CH<sub>4</sub>, CO, HCFC-22, H<sub>2</sub>O and N<sub>2</sub>O. For each month, latitude band and altitude a chemical box model has been run to calculate which fraction of the initial concentration was still present after one month. The following sink reactions were considered: Photolysis with TUV-based photolysis rates (Madronich and Flocke, 1998), and reactions with OH, O(<sup>1</sup>D), and atomic chlorine (Sander et al., 2010). For H<sub>2</sub>O and CO also source reactions were considered, namely methane oxidation and 80 photolysis of CO<sub>2</sub>, respectively. In cases where these source reactions outweigh the sinks, the monthly survival rate can be larger than unity. These box model calculations were performed offline and results were tabulated, allowing the ANCISTRUS code to operate with reasonably large time steps. For SF<sub>6</sub>, no sinks were considered. Since values at the upper boundary are



prescribed using MIPAS measurements, neglect of sinks above will not cause artificial ‘over-aging’ as described by Stiller et al. (2012b).

85 While in principle ANCISTRUS is designed to infer both effective 2D velocities and mixing coefficients, in the current version a regularization has been chosen to impose the mixing coefficients to be zero. This choice stabilizes the inversion although it does not provide full information on how mixing propagates onto the velocities. Thus the derived velocities have to be understood as the efficient 2D circulation velocities which best describe the redistribution of trace species, under the constraint that Fickian mixing makes no contribution.

## 90 2.2 MIPAS

The Michelson Interferometer for Passive Atmospheric Sounding (MIPAS; Fischer et al. 2008) is a Fourier transform infrared limb emission spectrometer on Envisat. The sun-synchronous polar orbit of the satellite, with an inclination of about 98.5°, allowed global measurements of trace gases with dense coverage. MIPAS was operational from July 2002 to April 2012, with some sizeable data gaps in 2004 and 2005. Due to a failure of the interferometer mirror slide in 2004, operation at high spectral  
95 resolution was stopped in March 2004. In January 2005 operation was resumed, however at degraded spectral resolution. This went along with an improvement of spatial sampling. The altitude coverage of useable tangent altitudes in the nominal measurement mode of MIPAS ranges from cloud top altitude to the middle mesosphere. Data products relevant to this study are temperature and H<sub>2</sub>O (von Clarmann et al., 2003, 2009), CH<sub>4</sub> and N<sub>2</sub>O (Plieninger et al., 2015), CFC-11, CFC-12 (Kellmann et al., 2012), HCFC-22 (Chirkov et al., 2016), CCl<sub>4</sub> (Eckert et al., 2017), SF<sub>6</sub> (Stiller et al., 2012b; Haenel et al., 2015), and  
100 CO Funke et al. (2009). The products have been widely validated, e.g., by Stiller et al. (2012a); Plieninger et al. (2016); Eckert et al. (2016), just to name a few.

## 2.3 The Climatology of middle atmospheric meridional circulation

From MIPAS measurements of the considered trace species monthly zonal mean distributions were calculated for latitude/altitude bins of 6°/3 km. Monthly distributions were available from July 2002 to April 2012 with data gaps in 2004, 2005  
105 and 2006. For each pair of subsequent months, two-dimensional circulation fields were calculated, using the ANCISTRUS-tool described above. This resulted in 89 circulation fields, the first representing August to September 2002, the latest March to April 2012. Then, all January-February fields were averaged, all February-March fields, etc., to form the 12-monthly climatology.

The use of language is not uniform in the community. For the description of the figures, we use the following terminology: The ‘overturning circulation’ we understand is the mesospheric pole to pole circulation, consisting of one single rotation cell  
110 and mainly driven by gravity wave breaking (Plumb, 2002; Dunkerton, 1978).

The ‘deep branch of the BDC’ is the circulation from the equator to the poles in the middle/upper stratosphere with uplift in the tropics and subsidence over the poles, (Plumb, 2002; Birner and Bönisch, 2011; Bönisch et al., 2011). For the transport pattern from the tropics to midlatitudes in the lower stratosphere we use the term ‘shallow branch of the BDC’.





### 3 Results

115 Figures 1–2 show the resulting circulation fields in the full altitude range from 6 to 68 km. We also show the circulation patterns  
only for altitudes 30 km (Figs. 3–4), where the reduced altitude range along with the reduced maximum velocities allows to  
better resolve the smaller effective velocities found in the UTLS and troposphere.

Since these monthly circulation patterns are built from averages covering the period August 2002 to April 2012, the following  
characteristic has to be kept in mind when interpreting these results. A strong circulation feature which appears in every year  
120 but not always exactly at the same latitude, altitude, or time appears weaker in these climatologies. Conversely, a weaker  
pattern, which appears every year at the same latitude, altitude, or time will appear stronger.

To diagnose this effect, also the standard deviations of the circulation vectors, which are a measure of their variability, are  
shown in Figs. 5–6.

#### 3.1 An average year of middle atmospheric circulation

##### 125 3.1.1 January-February

The circulation pattern inferred from the change of trace gas distributions from January to February shows two major circulation  
cells with opposite rotation (Fig. 1, upper left panel). In the Northern, local winter, hemisphere there is strong transport from the  
Southern tropics (up to 30°S) to the Northern subarctic latitudes, with maximum effective velocities in the upper stratosphere,  
between 40 and 45 km altitude. This can be associated with the upper branch of the BDC. Separated by a local minimum  
130 of effective velocities at 30 km altitude, there is a further branch of the Brewer-Dobson circulation in the lower to middle  
stratosphere. While its velocities and vertical extension are smaller, its contribution to the airmasses transported to higher  
latitudes is still significant due to the larger air density at these lower altitudes. The direct vertical motion over 30°S creates a  
sort of transport barrier to horizontal circulation for the 30–55 km altitude range.

Above 50 km at Northern polar latitudes there is some subsidence. Associated year-to-year variability is large, reflecting the  
135 irregular appearance of sudden stratospheric warmings (Figure 5, upper left panel). In the middle and lower Northern polar  
stratosphere there is no clear signal of subsidence. This can be explained by the fact that the northern polar vortex is known  
to be regularly displaced from the pole, which causes subsidence effects to be averaged out when latitudinal averages are  
considered. In equivalent latitudes this would look different but this representation would not be optimal for global analyses.

At the same time, we find in the SH a region of southward/poleward transport around 60 km altitude starting around 30°S,  
140 and subsidence over high Southern latitudes in the mesosphere and upper stratosphere. It would be bold to associate it with the  
Brewer-Dobson circulation, because measured temperature profiles suggest that the stratopause during this time is at about 50  
km. Instead, this is a mesospheric branch of an Equator-pole circulation. Most parts of the Southern hemispheric stratosphere  
are quite calm. Low variabilities indicate that this is a very typical condition. At Southern midlatitudes there is an isolated cell  
of pronounced poleward transport at tropospheric altitudes between 8 and 12 km (Fig. 3, top left panel). We associate this with  
145 the transition branch of the BDC reported by Lin and Fu (2013) and Diallo et al. (2019).

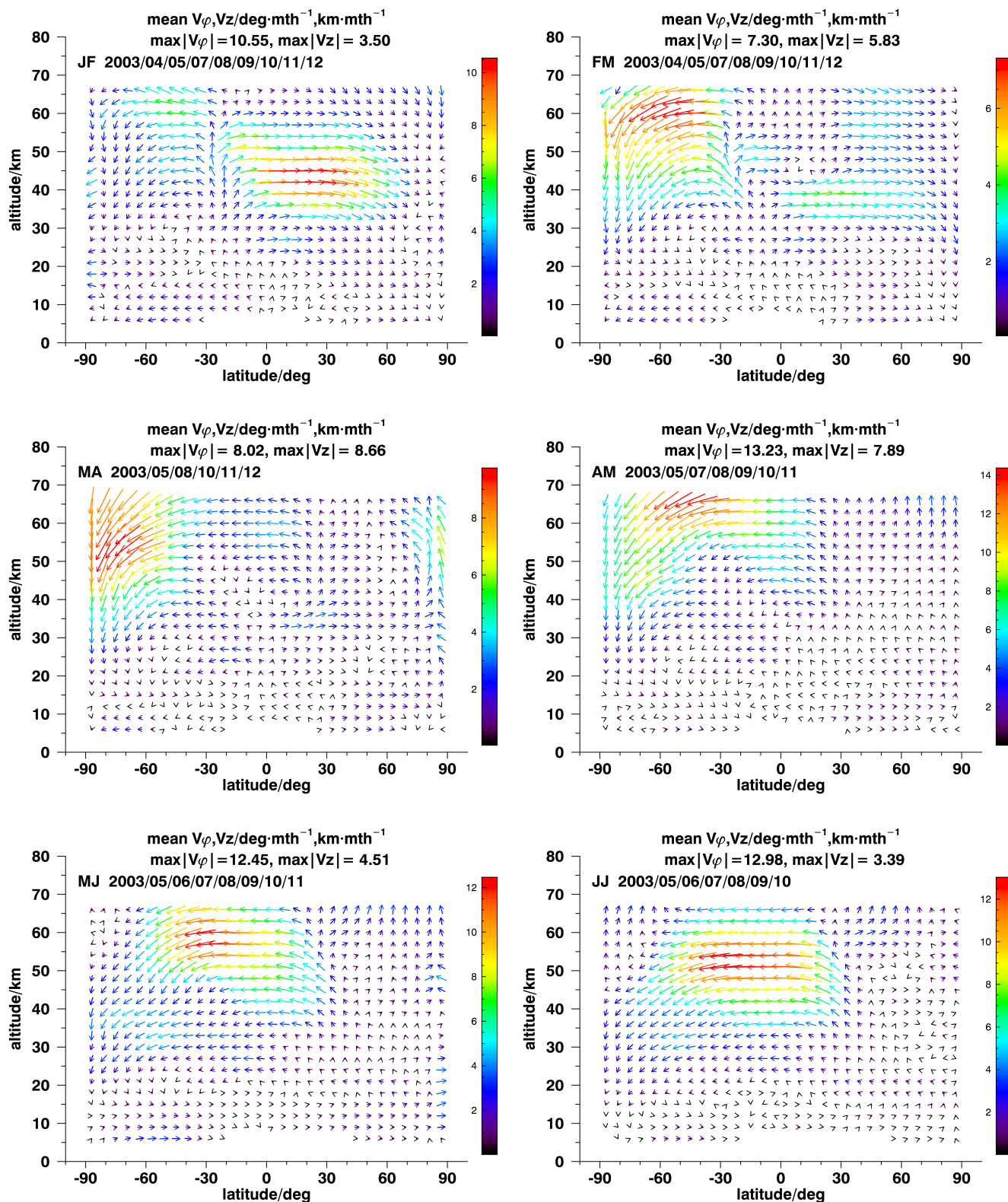


**Figure 1.** : Mean monthly circulation patterns from January–February (top left, JF) to June–July (bottom right, JJ). The headers give quantitative information about maximal effective velocities, the months and years considered. Note the different colour scales of the plots. The colour scales refer to  $\sqrt{(v_\phi \text{ deg}^{-1} \text{ mth})^2 + (v_z \text{ km}^{-1} \text{ mth})^2}$  for  $v_\phi$  and  $v_z$  in units of  $\text{deg mth}^{-1}$  and  $\text{km mth}^{-1}$ .

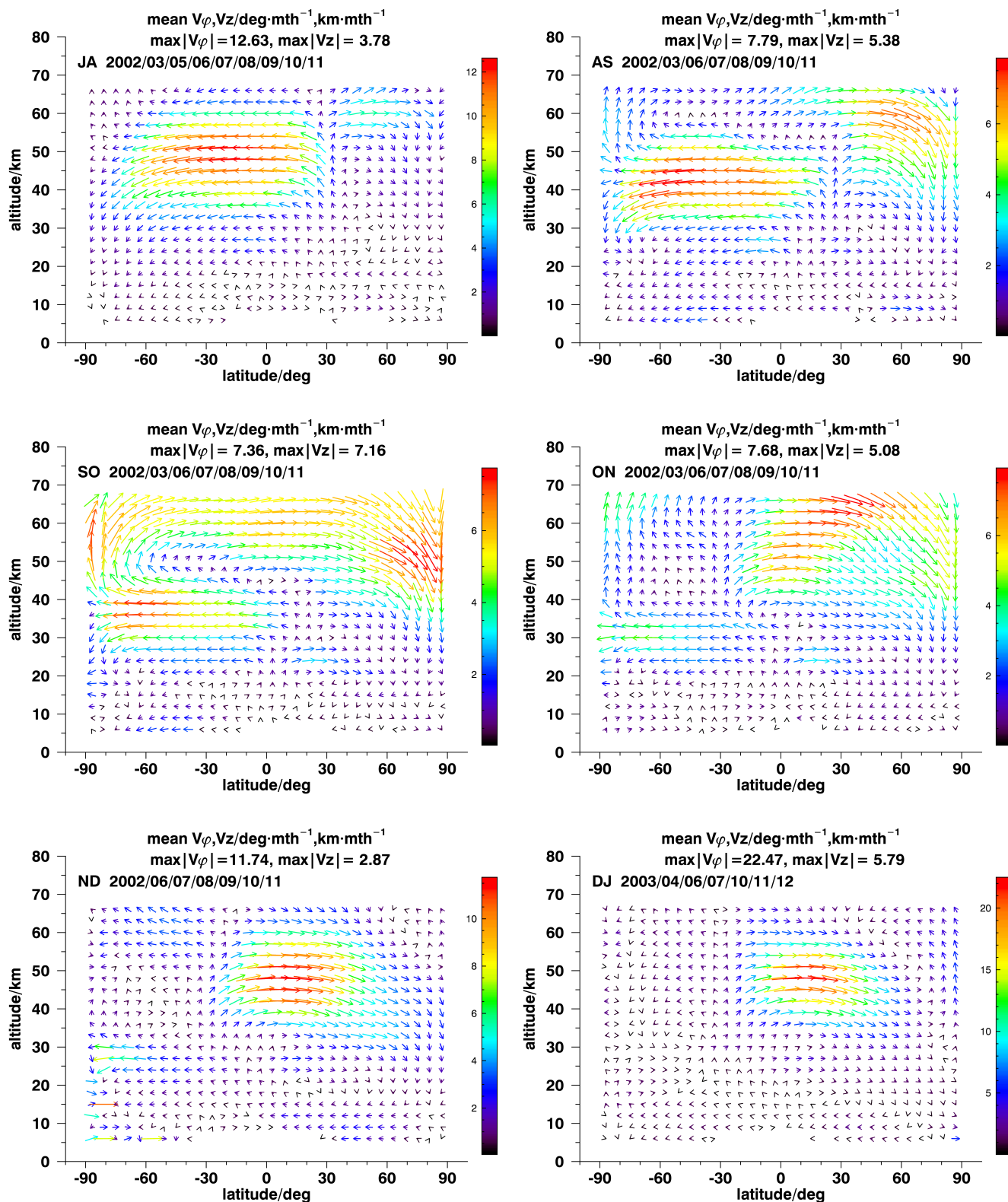


**Figure 2.** : Mean monthly circulation patterns from July–August (top left, JA) to December–January (bottom right, DJ). For details, see Fig. 1.

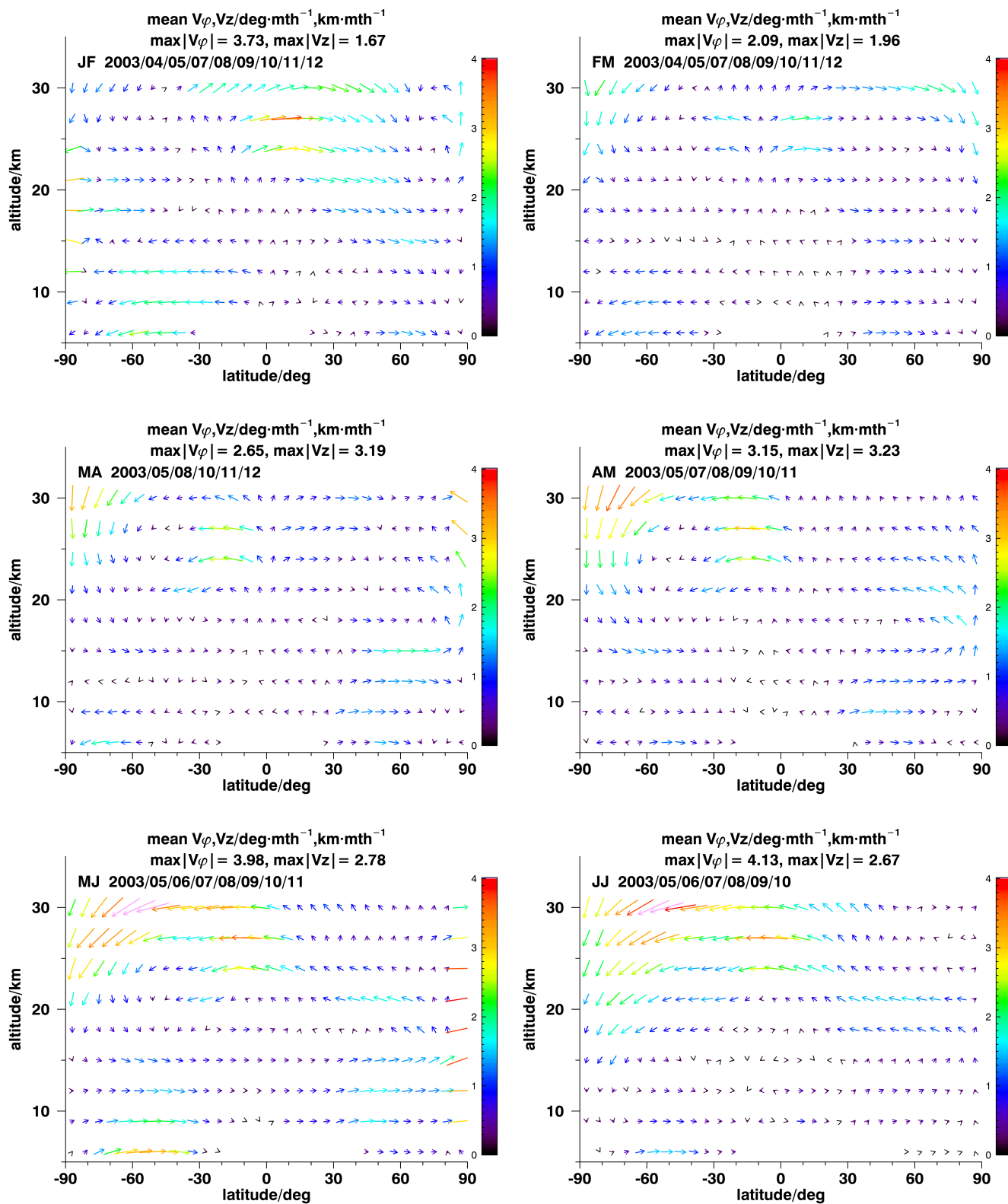


Figure 3. : Same as Fig. 1 but for altitudes up to 30 km only.

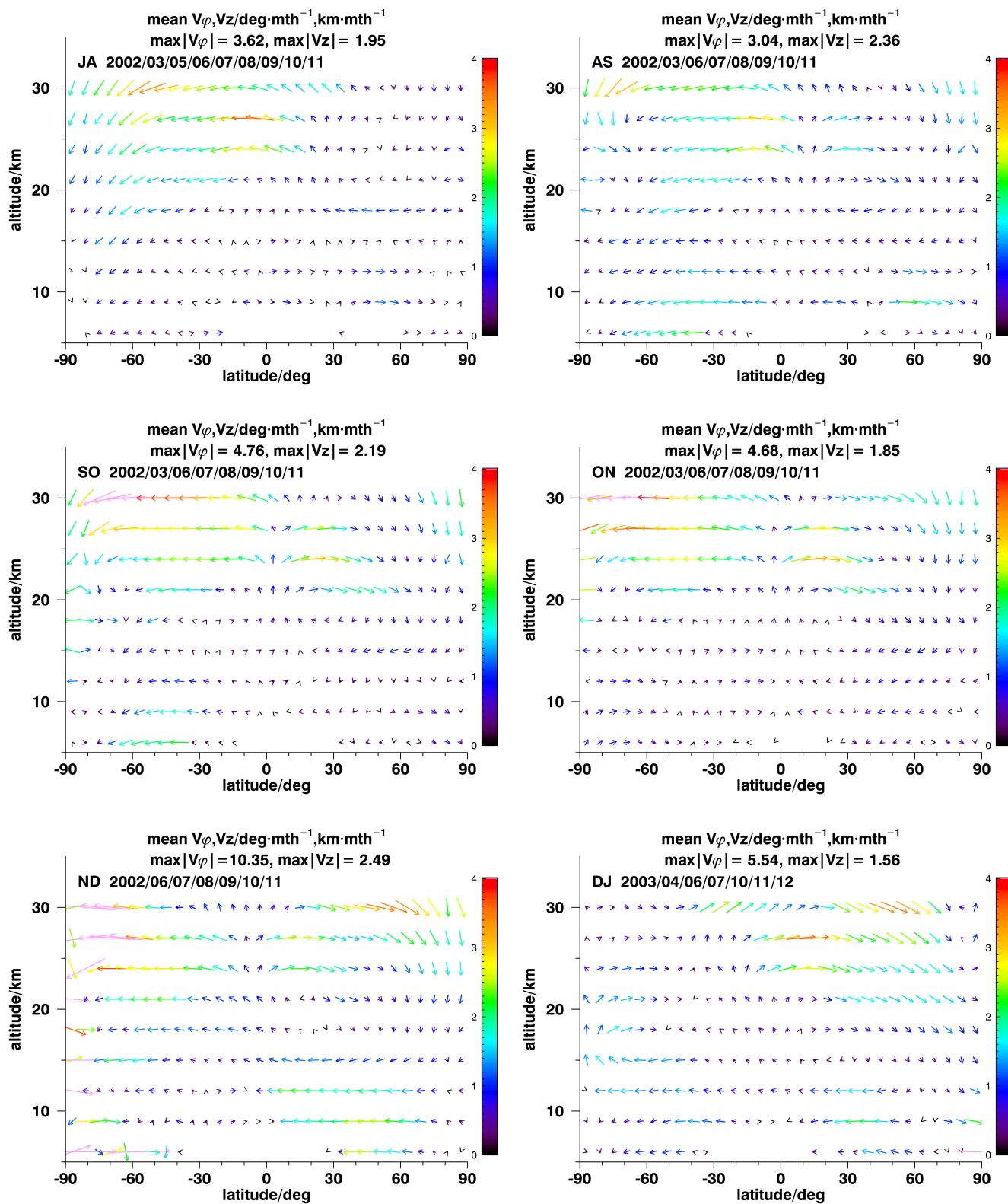
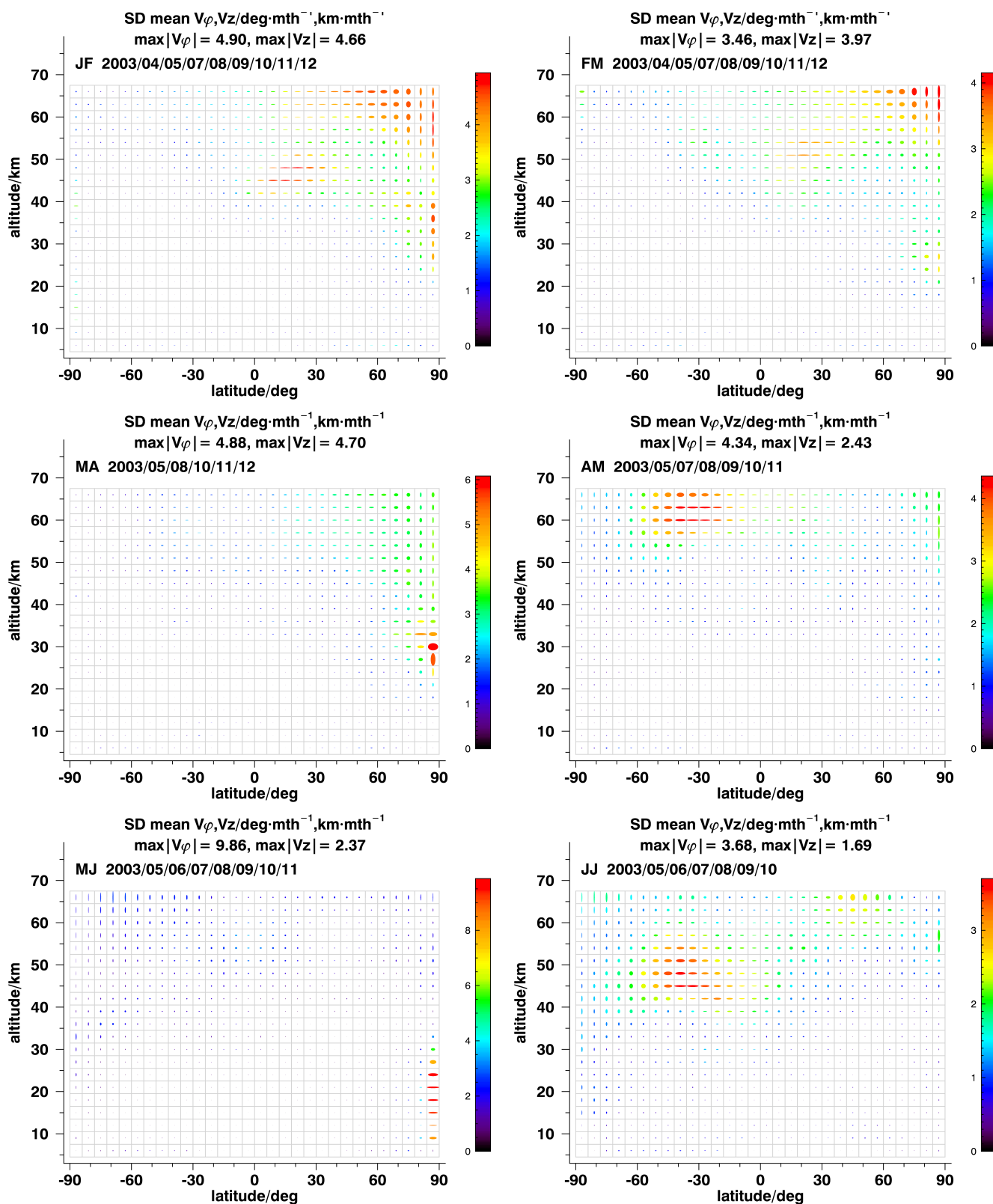
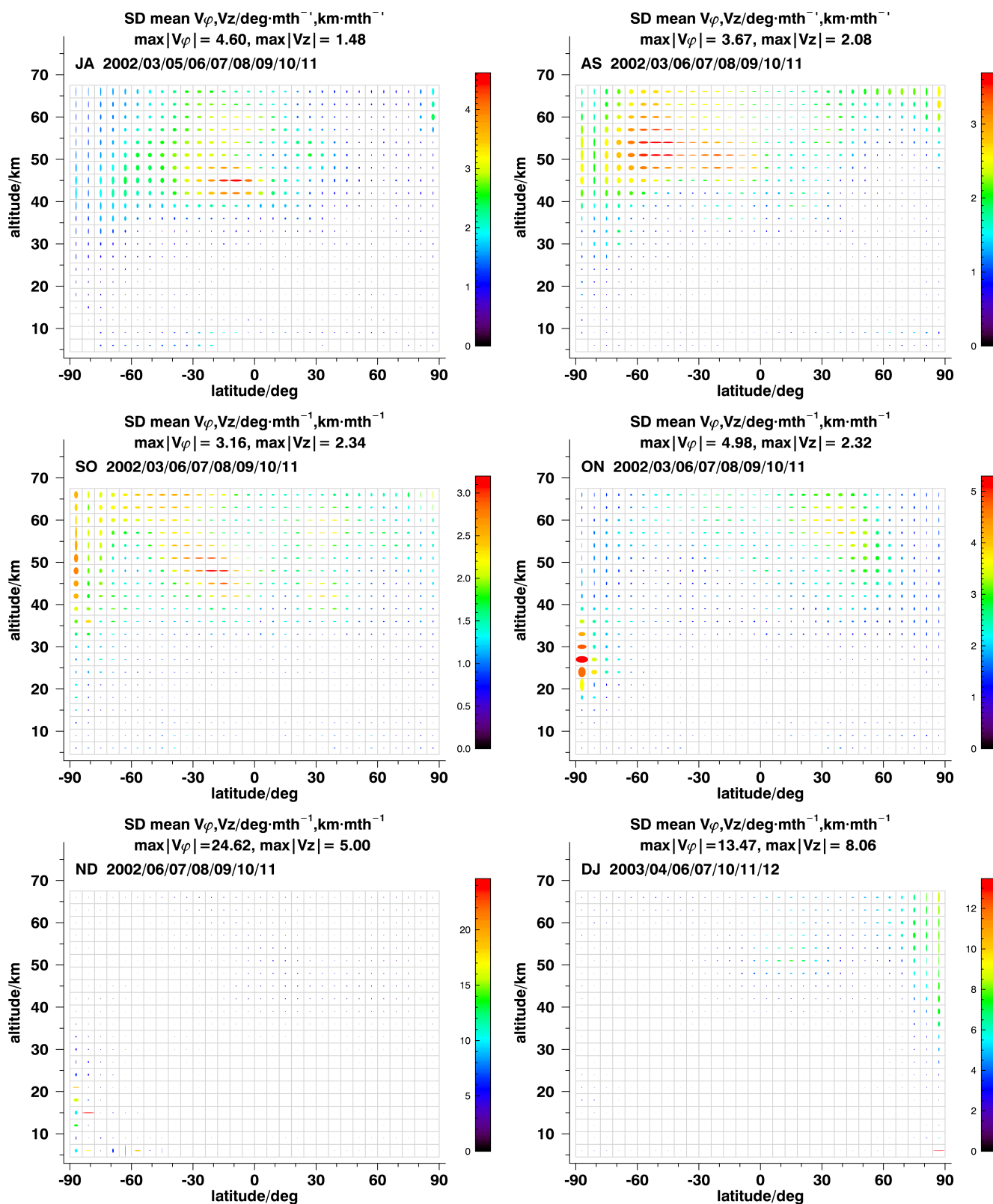


Figure 4. : Same as Fig. 2 but for altitudes up to 30 km only.



**Figure 5.** : Inter-annual variability of the middle atmospheric circulation in terms of standard variations from January–February (top left, JF) to June–July (bottom right, JJ). For details, see Fig. 1.





**Figure 6.** : Inter-annual variability of the middle atmospheric circulation in terms of standard variations from July–August (top left, JA) to December–January (bottom right, DJ). For details, see Fig. 1.





Tropical uplift, which separates the anti-parallel circulation patterns described above, has largest effective velocities at 50 km altitude and is situated at 30°S. At lower altitudes effective uplift velocities are small and maxima seem to be found further equatorward compared to higher altitudes. This leads to a warped tropical pipe.

In the altitude range covered by our data no indication of a pole to pole overturning circulation is seen.

150 Except for the highly variable subsidence at Northern polar regions, inferred velocities largely exceed their variabilities by a factor of 3, indicating that these results are robust and, due to only moderate year-to-year variability, are fairly representative for the atmospheric state at this time of the year.

### 3.1.2 February-March

The upper stratospheric transport pattern from the tropics to the North pole around 40 km has considerably weakened, and  
155 at least in the middle stratosphere (around 30 km) there is now a stronger signal of Northern polar subsidence (Fig. 1, right upper panel). The Southern hemispheric circulation pattern has become considerably stronger. Southern polar subsidence is more clearly pronounced than the month before and is seen to reach lower altitudes. Effective velocities decrease towards lower altitudes which is an immediate and expected effect of increasing air density during subsidence. The NH middle stratospheric poleward circulation pattern below 30 km remains intact, and a Southern hemispheric counterpart has emerged. The deep  
160 branch of the BDC starts to form from the tropical region above 20 km.

Roughly following the seasonal movement of the solar zenith, the tropical pipe has moved slightly towards the equator. Between 40 and 45 km there is still a poleward offset of the latitudinal region of uplift which separates the northern and southern circulation patterns at 18°S. Between 45 and 55 km the upward movement bifurcates into a Northern and Southern transport branch. The Northern one feeds into a mesospheric circulation pattern that exists above the deep branch of the BDC  
165 (at 55 km and above), while the Southern branch feeds into the dominating circulation pattern of the SH upper stratosphere and mesosphere. At 55 km a reverse offset of the latitude of strongest uplift is observed towards northern latitudes. This movement will proceed further in the following months and will give rise to a mesospheric overturning pole-to-pole circulation later in the year.

Shallow branches of the BDC are seen in both hemispheres. In northern midlatitudes this pattern extends higher up into the  
170 stratosphere while in the southern hemisphere (SH) it is confined to the lowermost stratosphere. Arguably, the classification of this feature as the lower branch of the BDC is not straightforward because it is not clear enough whether this feature is fed by the tropical uplift. In the lower southern midlatitude stratosphere there is even an altitude region (~ 15 km) where equatorward backflow is observed which possibly closes the loop of the circulation above.

Again the regions of large variability are confined to high Northern polar latitudes and a small region at 53 km altitude, 26°  
175 latitude. This again shows moderate year-to-year variability and representative results elsewhere.

### 3.1.3 March-April

An overturning circulation feature forms which is also fed by tropical air above about 30 km (Fig. 1, left middle panel). The uplift barrier between 40 and 60 km has moved to 30°N and makes this overturning circulation feature bifurcate into



two branches, one developing into the deep pole-to-pole circulation above 65 km, and another one from the tropics to the southern high latitudes below 65 km. In the SH, a deep BDC branch has clearly developed from the subtropical pipe cell above 20 km (Fig. 3), and adds poleward and subsidence motion to the overturning circulation branch over the Southern Pole. This subsidence reaches further down than in the preceding month. At 15 km altitude there is some back-flow of southern polar air towards lower latitudes.

In the NH, the overturning circulation seems to be fed from a second altitude region. Besides the deep branch of the BDC around 35 km, poleward transport in the lower stratosphere (10 - 15 km) from the subtropics (30°N) to the high latitudes is feeding into the uplift over the North Pole as well. Above 15 km the arriving air is uplifted, while air arriving at lower altitudes subsides (Fig. 3, middle left panel).

The structure of circulation over the NH midlatitudes leaves an isolated region between 35°N-65°N in the altitude range of 30-65 km without a sizeable vertical velocity component (Fig. 1). This seems to contribute to the formation of the uplift latitudinal barrier that will appear around 60°N in the following months.

Large variability in the lower stratosphere in high northern latitudes (Fig. 5, middle left panel) is attributed to late winter vortex dynamics.

#### 3.1.4 April-May

In the southern polar stratosphere there is still strong subsidence (Fig. 1, right middle panel). Maximum velocities have shifted higher up (around 70 km) and towards lower latitudes. The northern polar uplift branch of the mesospheric overturning circulation has also moved upwards and broadened so that it covers NH middle and high latitudes now. It does not show the tropical origin anymore, i.e., this part of the pole-to-pole circulation branch is now disconnected from the tropical pipe. Instead, a strong transport branch from the Northern subtropics (30°N) to the South Pole has developed for altitudes above 40 km. This transport path avoids the detour over the Northern polar latitudes but feeds into the mesospheric circulation at about 30°N.

In the Northern lower stratosphere between 10 and 25 km a circulation has established with poleward transport below 15 km and upward and southward transport between 15 and 25 km (see Fig. 3, middle right panel). In the SH there exists a second transport branch from the equator to subarctic latitudes between 20 and 30 km, the deep branch of the BDC, that has strengthened compared to the previous month (see Fig. 3, middle right panel). As in the preceding month, some back-flow of polar air towards low latitudes is detected in the SH at 15 km, most pronounced in sub-polar regions. Large interannual variability is observed above 55 km at SH mid and lower latitudes (Fig. 5, middle right panel), related to the varying vertical extent of the pole-to-pole overturning circulation.

#### 3.1.5 May-June

The mesospheric branch of the BDC in the SH is still there, now with maximum velocity shifted towards subtropical latitudes and lower altitudes (Fig. 1, lower left panel); this circulation branch now causes subsidence over SH midlatitudes at higher levels. At about 30–40 km descending air encounters the lower deep branch of the BDC. Air is further transported towards the polar region where these merged branches of the BDC result into subsidence. While in the preceding month subsidence over



the Antarctic was observed up to the highest altitudes, now the circulation above 60 km starts to reverse, which will lead to a south-north pole-to-pole circulation in the next six months. There is indication of a reversal of the shallow branch in the SH with strongly increased equatorwards transport velocities (compared to the previous month) in the range below 15 km.

215 Again, the NH is quite calm in terms of absolute velocities but the circulation of air with transport towards the pole below 15 km and back to the mid-latitudes and subtropics around 20 km has strengthened (Fig. 3, lower left panel). The region of vertical transport around 30°N has moved down to altitudes between 30 and 50 km. Vertical uplift in between 40°N - 60°N in the altitude range of 40-60 km feeds the SH mesospheric circulation branch.

### 3.1.6 June-July

220 A clear pattern of the deep branch of the BDC has established in the SH, with transport from the Northern subtropics (35°N) to the South Pole and subsidence there below 40 km (Fig. 1, lower right panel). Relatively large variability in the range of 30° - 60° S and 45 to 55 km altitude indicates that the extent of high transport velocities towards the South Pole varies from year to year (Figure 5, lower right panel). A very weak backward flow to the equator is present below 13 km (Fig. 3, lower right panel). The southern polar uplift now starts already at 50 km altitude. It will intensify during the following months. Eventually,  
225 three months later, it will form the upwelling branch of the overturning pole-to-pole circulation.

The middle to upper stratosphere in the NH is rather quiet. Some uplift is still present in midlatitudes above 55 km that is fed from the subtropical region (30°N). An area of uplift from 25-50 km above 30°N forms a horizontal transport barrier in the sense that air southward of this barrier is transported in direction to the South Pole; this feature persists until August-September.

The circulation pattern in the lower Northern stratosphere is still present. The poleward transport in the lower branch as  
230 observed the month before has weakened. Now we observe an upwelling pattern from 30-40°N that transports air upwards and polewards up to around 75°N before turning towards the tropics at about 20 km altitude (Fig. 3, lower right panel). This feature is also observed in the following month, but loses strength in August-September, when this pathway is overpowered by the descent of the already forming overturning circulation in the Northern Hemisphere (NH) high latitudes. The low standard deviations corresponding to this region and time of the year indicate that this is the usual path tracers follow (Fig. 5, lower  
235 right panel.). This, together with the lack of a SH counterpart, allows us to link this pattern to the occurrence of the Asian Monsoon, which has been recently shown to be an effective pattern for transport of tropospheric tracers into the stratosphere (e.g. Randel et al., 2010; Ploeger et al., 2017; Yu et al., 2017). Our results show overall agreement with the one shown by Ploeger et al. (2017). Differences related to the transport of tracers during the monsoon period can be attributed to the different time resolution in our study and theirs.

### 240 3.1.7 July-August

In general, the circulation patterns resemble those of the previous month, although shifted towards lower altitudes (Fig. 2, upper left panel). The only exception is the uplift barrier at 30°N which is displaced to higher levels. The circulation branch above 50 km from 30°N to the poles is strengthening. While in the previous month it seemed to feed chiefly the overturning pole-to-pole circulation, it now establishes the onset of northern polar subsidence, which will continue to gain importance



245 during the subsequent months. That is to say, what looked like overturning circulation the month before becomes more and more a BDC-like symmetric feature. The maximum updraft is located at  $30^{\circ}\text{N}$ . In the second half of the year, the patterns observed during the first six months are largely mirrored to the other hemisphere, however shifted in altitude, and the transport velocities are somewhat larger. The July-August patterns resemble widely the mirrored patterns seen in JF (Fig. 2, upper left panel). The pronounced deep branch of the BDC resides in the middle to upper stratosphere of the SH (35 to 60 km). A zone  
250 of vertical transport around  $30^{\circ}\text{N}$  and between 30 and 55 km forms a horizontal transport barrier. Above this barrier, upward and poleward transport with a source region in the Northern subtropics has established. Indication of uplift over the South Pole is seen above 60 km.

The circulation pattern in the Northern lower stratosphere with poleward transport below 15 km and equatorward transport around 20 km is still existent. As in the previous months we assign this circulation cell to the NH monsoon systems (Fig. 4,  
255 upper left panel).

Variability in the upper stratosphere over tropics and southern midlatitudes is larger than the NH counterpart in January-February (Fig. 6, upper left panel). Although small, there is a sizeable variability in vertical velocity over the South pole related to year-to-year variability of the descent inside the polar vortex.

### 3.1.8 August-September

260 The general circulation pattern resembles that of the preceding month (Fig. 2, upper right panel). However, the maximum of peak velocities of the SH circulation branch are now found at lower altitudes. A bifurcation of the circulation is found near the southern polar stratopause. This poleward circulation branch around 45 km altitude feeds both the mesospheric overturning circulation which now has established in south north direction, and the southern polar subsidence. In the northern polar upper stratosphere and mesosphere strong poleward transport and subsidence starts to establish, which is fed by the mesospheric  
265 overturning circulation, by tropical uplift south of  $30^{\circ}\text{N}$  from above 55 km, and by Northern mid-latitude air from 35 to 55 km. Meridional velocities in the winter hemisphere are stronger in the  $0\text{-}70^{\circ}\text{S}$ , 40 km altitude range in August-September compared to the NH counterpart in February-March.

In the lowermost stratosphere, we see isolated shallow branches of the BDC below 15 km transporting air from the subtropics to the poles in both hemispheres (Fig. 4, upper right panel). Similar to February-March and March-April, vertical transport is  
270 present over the equator up to about 27 km; this vertical transport feeds into two rather weak circulation cells in midlatitudes below 25 km. In the SH this circulation merges with the poleward transport further down, while in the NH, the circulation merges with the weakened equatorward transport around 20 km that was observed in the previous months.

We can see a reversal in the horizontal velocities in the NH lower stratosphere above about 10 km from around  $40^{\circ}\text{N}$  to the equator. We associate this with Asian-monsoon-related transport.

### 275 3.1.9 September-October

The circulation in September-October is dominated by a pronounced overturning pole-to-pole circulation feature, being lower in altitude than its boreal spring counterpart (Fig. 2, middle left panel). All transport above 55 km is directed upwards and



280 towards the North Pole. The deep branch cell of the BDC in the SH observed in the previous months has moved further down (25 to 40 km) and further polewards and feeds, by bifurcation, into the overturning circulation in its upper part. The lower part still feeds into the subsidence area in the middle to lower South polar atmosphere (below 30 km). The uplift region that forms a horizontal transport barrier is now located between 25 and 40 km and closer to the equator, at about 20°N. Above this barrier, all transport in the NH is directed towards the North Pole. A second region of purely vertical transport is found directly above the equator between 20 and 30 km. This region of vertical transport separates two weak circulation cells in both hemispheres. The SH one merges with the deep branch of the BDC, while the NH counterpart provides poleward and downward transport  
285 towards 60°N and then turns into equatorward transport around 15 to 20 km. In the lowermost stratosphere and UTLS (below 13 km, Fig. 4, middle left panel) we observe some poleward transport in the SH while the NH atmosphere in this altitude range is rather quiet.

### 3.1.10 October-November

The transport cell related to the deep branch of the BDC in the SH has weakened considerably, and has shrunk and moved  
290 further down to 25 to 35 km (Fig. 2, middle right panel). Although its upper part still feeds into the uplift over the South Pole, it is now more separated from the above regions and more clearly causing also air descent over the South Pole.

The horizontal transport barrier formed by vertical transport has jumped back to the SH and is located around 30°S from this month on (until March-April). Its altitude range is again 45 to 65 km. It creates an isolated region at 40° – 60°S and 40-55 km, similar to the one found in the NH during March-April, although smaller now. All transport above 40 km and northward of  
295 30°S is directed towards the North Pole and leads to subsidence there. Increased upward velocities over the South Pole above 55 km indicate the existence of an overturning mesospheric pole-to-pole circulation, but this seems to take place at altitudes mainly above 68 km and can thus not be diagnosed here. In contrast, a tropical feeding of the former overturning circulation takes over and will develop in the subsequent month into the deep branch of BDC in the NH. A second region of purely vertical transport is present over the equator between 20 and 30 km and acts as horizontal transport barrier there. It is flanked by a weak  
300 NH circulation cell transporting air into midlatitudes above 20 km and equatorwards below 15 km. (Fig. 4, middle right panel).

Largest variability at 20 to 35 km over the South pole is related to interannual variations in the timing of the SH polar vortex break-up, associated with the high values seen in Figure 6, middle right panel. This had already started in the previous month in the upper stratosphere.

### 3.1.11 November-December

305 The most pronounced feature in this month is the deep branch cell of the BDC in the NH at very high altitudes (35 to 60 km), transporting air from the Southern subtropics (30°S) to the North Pole (Fig. 2, lower left panel). Subsidence over the winter pole is present below 50 km. Some upward and Southern poleward transport is present over the SH midlatitudes above 55 km, similar to the May-June and June-July situation in the NH. A very weak remnant of the deep branch of the BDC is present in the SH between 20 and 30 km. In the lowermost stratosphere, a reversal of the shallow branch of the BDC with transport



310 towards the equator can be seen (Fig. 4, lower left panel). This is especially clear for the NH. This equatorward transport seems to be fed by the subsidence over the North pole. A similar but weaker feature was observed in the SH in March-April.

### 3.1.12 December-January

The deep branch of the BDC is still seen as the main circulation feature near the Northern tropical and midlatitudinal stratopause. However, it has shrunk in latitudinal extension and feeds the subsidence over the North Pole only below 25  
315 km (Fig. 2, lower right panel). In the northern polar upper stratosphere the vertical velocity has reversed, showing upward velocities. Interannual variability, however, is high here, probably caused by frequent sudden stratospheric warmings appearing at different times of the NH winter (Figure 6, lower right panel). In the shallow branch of the BDC, equatorward transport in the NH midlatitudes below 15 km and poleward transport in the SH at the same altitude range is present. In the SH, the circulation pattern is closed by upward and equatorward transport in the 15 to 25 km region (Fig. 4, lower right panel).

## 320 3.2 Summary

We have presented here a new climatology of middle atmospheric circulation fields, derived from long-lived tracer measurements from MIPAS. The climatologies have been constructed from independent ANCISTRUS results (von Clarmann and Grabowski, 2016) with a latitudinal/vertical resolution of 6°/3km; resulting fields are stable over the years of the MIPAS mission (2002–2012). This both increases confidence in the robustness of the analysis method and shows that the patterns displayed  
325 are indeed typical phenomena of the middle atmospheric circulation, which remain after the calculation of the multi-year averages. Other phenomena, which also appear on a regular basis but vary in the exact latitude or time where/when they appear, average out. This issue is further discussed in Section 3.2.3. In the following, we present a synopsis of the main phenomena found.

### 3.2.1 The BDC and the Overturning Circulation

330 The upper branch of the BDC and the overturning pole-to-pole circulation are not, according to our data, two independent phenomena but we observe quite smooth transitions between both. While from July to September there are still two major, roughly antiparallel circulation cells below 68 km, in September-October we have one single northward circulation pattern above 50 km. Our data are consistent with the assumption - but do not directly support it - that from March to May there exists a southward pole to pole circulation which is situated at altitudes not covered by MIPAS data.

335 From our data, the direct uplift of air from the tropopause above the equator seems not to be the preferred tracers' path in shorter timescales. Such tropical uplift is clearly seen only in January-February and October-November. On the other hand, this uplift is known to be slow and robust in a statistical sense. This suggests that the tropical pipe may not be an actual transport path but instead a residual which emerges when fluctuations at shorter timescales cancel out.



### 3.2.2 Inter-hemispheric Differences

340 While we see corresponding features in the SH and NH, NH atmospheric circulation is not merely a mirrored southern hemi-  
spheric circulation phase-shifted by six months. The main differences are:

1. The deep branch of the BDC in the local winter stratosphere is stronger in the SH than in the NH.
2. While the major patterns can be found in both hemispheres, their typical altitude is different in the NH compared to the  
345 SH. Overall, they appear at higher levels in the SH. This applies for instance to the low-midlatitudes feature in May-June  
and June-July in the SH, and in November-December and December-January feature in the NH. Another example is the  
overturning circulation feature in March-April in the SH and September-October in the NH.
3. The location of vertical uplift separation barriers is different in both hemispheres.
4. There are differences in the structure of the overturning circulation: only one pathway is observed in the SH towards NH  
350 branch in September-October while two pathways are seen in the NH towards SH branch in March-April. This creates a  
large region of isolated air in the NH for these months, without a SH counterpart.
5. In the NH we detect a summer signal (June to September), that has no SH counterpart, which we attribute to the Asian  
monsoon.

### 3.2.3 Variable Phenomena

The variability of atmospheric transport is largest at winter polar latitudes. This applies both to the lower mesosphere/upper  
355 stratosphere region and the middle stratosphere (Figs. 5–6). In the NH this variability is related to sudden stratospheric warm-  
ings. This variability causes an underrepresentation of the related transport pattern in the climatology. Conversely, in the SH, the  
interannual variability in the polar vortex break-up is associated with very high variability in transport in October–November  
in the SH polar region between 20–35 km, as this is also affecting the highest latitude the deep branch of the BDC can reach.

Another region of large variability is found over mid-low latitudes in the winter hemisphere (Figs. 5–6, January–February  
360 in the NH, June–July and July–August in the SH), reaching maximum standard deviation values between 40–50 km of altitude.  
In the SH this high variability pattern persists also in August–September and September–October. A further region of large  
variability appears in August–September above 45 km, centred around 50°S and is associated with the same circulation pattern.

## 4 Discussion and Conclusion

The ANCISTRUS method applied to MIPAS data reproduces well the known atmospheric meridional circulation patterns.  
365 Beyond this, additional information has been obtained from this new climatology regarding how some of these patterns evolve  
over the year. Compared to established methods, it provides circulation fields at largely improved temporal and spatial resolu-  
tion and at altitudes not accessible by the classical methods such as age-of-air analysis on the basis of air sampling instruments





of satellite based SF<sub>6</sub> measurements. The results are stable in a sense that the interannual variability of a pattern seen at a certain time of the year is small, that is to say, the patterns do not average out when the mean circulation is calculated although the input circulation patterns for the averaging process have been generated independently. No common a priori velocity distribution has been used to push the results towards the expected circulation patterns. Furthermore, transitions between the circulation patterns of subsequent months are reasonably smooth, which is another indicator of the robustness of the results. Large interannual variability is mainly limited to situations where it can be explained by processes known to have large interannual variability in themselves, e.g. sudden stratospheric warmings.

The main features seen in these climatology fields are that the upper branch of the BDC and the overturning pole-to-pole circulation are heavily intertwined phenomena; the latitude of stratospheric uplift in the middle and upper stratosphere is more variable than previously established; and the schematics of the BDC usually shown (e.g. Fig. 1 of Bönisch et al. 2011) seem to be representative for certain months only, actually rather spring/autumn months instead summer/winter months as indicated in their figure, and do not capture enough detail and interactions between the various circulation branches.

Oncoming future steps consist in the application of this method to data from other space missions, like the Microwave Limb Sounder (MLS) on the Aura satellite (Waters et al., 2006) and the distinction of transport versus mixing. Researchers optimistic with respect to funding issues even plan an ANCISTRUS model in other than geometric altitude coordinates or even a three-dimensional version of ANCISTRUS, which would be a very versatile tool to infer velocities from concentration distributions for various applications.

## Appendix A: The interpretation of ‘effective velocities’

The effective velocities presented in this study cannot be interpreted as zonal mean velocities. The reason is twofold.

First, due to possible correlations between velocities and mixing ratios, products of prime terms in the zonal mean of the Reynolds decomposition of the tendency formulation of the continuity equation do not cancel out. Following Tung (1982)<sup>2</sup> and applying approximations suggested therein, von Clarmann and Grabowski (2016, Appendix A) rewrite the continuity equation

as

$$\frac{\partial \overline{\text{vmr}_g}}{\partial t} = -\frac{v^*}{r} \frac{\partial \overline{\text{vmr}_g}}{\partial \phi} - w^* \frac{\partial \overline{\text{vmr}_g}}{\partial z} + \frac{1}{r^2} \frac{\partial}{\partial \phi} \left[ K_\phi^* \frac{\partial \overline{\text{vmr}_g}}{\partial \phi} \right] + \frac{\partial}{\partial z} \left[ K_z^* \frac{\partial \overline{\text{vmr}_g}}{\partial z} \right], \quad (\text{A1})$$

where, contrary to the notation of the main text, velocities, mixing coefficients and state variables with a bar indicate zonal averages while quantities without a bar indicate longitudinally resolved quantities, and where

$$v^* = \overline{v} - \frac{1}{\overline{\rho}} \frac{\partial \overline{\rho' \eta'}}{\partial t} - \frac{1}{\overline{\rho r}} \frac{\partial \overline{\rho}}{\partial \phi} K_{\phi\phi} - \frac{\partial}{\partial z} K_{z\phi} - \frac{1}{\overline{\rho}} \frac{\partial \overline{\rho}}{\partial z} K_{z\phi}, \quad (\text{A2})$$

$$w^* = \overline{w} - \frac{1}{\overline{\rho}} \frac{\partial \overline{\rho' \Phi'}}{\partial t} - \frac{1}{\overline{\rho}} \frac{\partial \overline{\rho}}{\partial z} K_{zz} - \frac{1}{r} \frac{\partial}{\partial \phi} K_{\phi z} - \frac{1}{\overline{\rho r}} \frac{\partial \overline{\rho}}{\partial \phi} K_{\phi z}, \quad (\text{A3})$$

<sup>2</sup>There exist other approaches than that of Tung (1982) to interpret 2D circulation, using different approximations. Depending on the approach chosen, the calculation of effective 2D velocities from 3D fields involves different terms.



$$K_{\phi}^* = K_{\phi\phi}, \quad (\text{A4})$$

and

$$400 \quad K_z^* = K_{zz}, \quad (\text{A5})$$

$$K_{\phi\phi} = \frac{1}{\rho} \overline{(\rho v)' \eta'}, \quad (\text{A6})$$

$$K_{zz} = \frac{1}{\rho} \overline{(\rho w)' \Phi'}, \quad (\text{A7})$$

$$K_{\phi z} = \frac{1}{\rho} \overline{(\rho v)' \Phi'}, \quad (\text{A8})$$

405 and where  $\eta'$ ,  $\Phi'$  and  $\sigma'$  are defined by

$$\left( \frac{\partial}{\partial t} + \frac{\bar{u}}{r \cos \phi} \frac{\partial}{\partial \lambda} \right) \eta' = v', \quad (\text{A9})$$

$$\left( \frac{\partial}{\partial t} + \frac{\bar{u}}{r \cos \phi} \frac{\partial}{\partial \lambda} \right) \Phi' = w', \quad (\text{A10})$$

and

$$\left( \frac{\partial}{\partial t} + \frac{\bar{u}}{r \cos \phi} \frac{\partial}{\partial \lambda} \right) \sigma' = S'. \quad (\text{A11})$$

410 To generate effective quantities comparable to our results from 3D fields requires not only the calculation of the zonal mean velocities but also the evaluation of the second to fifth terms of Equations (A2) and (A3).

The second reason why our results cannot be understood as zonal mean velocities is that in our inversion we constrain to zero the effective mixing terms  $\frac{1}{r^2} \frac{\partial}{\partial \phi} \left[ K_{\phi}^* \frac{\partial}{\partial \phi} \overline{v m r_g} \right]$  and  $\frac{\partial}{\partial z} \left[ K_z^* \frac{\partial}{\partial z} \overline{v m r_g} \right]$ , i.e., those terms in the continuity equation (Eq. A10 in von Clarmann and Grabowski 2016) which act upon second derivatives of state variables. Thus, their effect is aliased onto

415 our effective velocities.



## References

- Andrews, A. E., Boering, K. A., Daube, B. C., Wofsy, S. C., Hints, E. J., Weinstock, E. M., and Bui, T. P.: Empirical age spectra for the lower tropical stratosphere from in situ observations of CO<sub>2</sub>: Implications for stratospheric transport, *J. Geophys. Res.*, 104, 26,581–26,595, 1999.
- 420 Birner, T. and Bönisch, H.: Residual circulation trajectories and transit times into the extratropical lowermost stratosphere, *Atmos. Chem. Phys.*, 11, 817–827, <https://doi.org/10.5194/acp-11-817-2011>, 2011.
- Bönisch, H., Engel, A., Birner, T., Hoor, P., Tarasick, D. W., and Ray, E. A.: On the structural changes in the Brewer-Dobson circulation after 2000, *Atmos. Chem. Phys.*, 11, 3937–3948, <https://doi.org/10.5194/acp-11-3937-2011>, 2011.
- Brewer, A. W. and Dobson, G. M. B.: Evidence for a world circulation provided by measurements of helium and water vapour distribution  
425 in the atmosphere, *Quart. J. Roy. Meteorol. Soc.*, 75, 351–363, 1949.
- Butchart, N., Scaife, A. A., Bourqui, M., de Grandpre, J., Hare, S. H. E., Kettleborough, J., Langematz, U., Manzini, E., Sassi, F., Shibata, K., Shindell, D., and Sigmond, M.: Simulations of anthropogenic change in the strength of the Brewer-Dobson circulation, *Clim. Dyn.*, 27, 727–741, <https://doi.org/10.1007/s00382-006-0162-4>, 2006.
- Chirkov, M., Stiller, G. P., Laeng, A., Kellmann, S., von Clarmann, T., Boone, C., Elkins, J. W., Engel, A., Glatthor, N., Grabowski, U.,  
430 Harth, C. M., Kiefer, M., Kolonjari, F., Krummel, P. B., Linden, A., Lunder, C. R., Miller, B. R., Montzka, S. A., Mühle, J., O’Doherty, S., Orphal, J., Prinn, R. G., Toon, G., Vollmer, M. K., Walker, K. A., Weiss, R. F., Wiecele, A., and Young, D.: Global HCFC-22 measurements with MIPAS: retrieval, validation, global distribution and its evolution over 2005–2012, *Atmos. Chem. Phys.*, 16, 3345–3368, <https://doi.org/10.5194/acp-16-3345-2016>, 2016.
- Diallo, M., Legras, B., and Chédin, A.: Age of stratospheric air in the ERA-Interim, *Atmos. Chem. Phys.*, 12, 12 133–12 154,  
435 <https://doi.org/10.5194/acp-12-12133-2012>, 2012.
- Diallo, M., Konopka, P., Santee, M. L., Müller, R., Tao, M., Walker, K. A., Legras, B., Riese, M., Ern, M., and Ploeger, F.: Structural changes in the shallow and transition branch of the Brewer–Dobson circulation induced by El Niño, *Atmos. Chem. Phys.*, 19, 425–446, <https://doi.org/10.5194/acp-19-425-2019>, 2019.
- Dobson, G. M. B.: Origin and distribution of polyatomic molecules in the atmosphere, *Proc. R. Soc.*, A236, 187–193, 1956.
- 440 Dunkerton, T.: On the mean meridional mass motions of the stratosphere and mesosphere, *J. Atmos. Sci.*, 35, 187–193, [https://doi.org/10.1175/1520-0469\(1978\)035<2325:OTMMMM>2.0.CO;2](https://doi.org/10.1175/1520-0469(1978)035<2325:OTMMMM>2.0.CO;2), 1978.
- Eckert, E., Laeng, A., Lossow, S., Kellmann, S., Stiller, G., Clarmann, T., Glatthor, N., Höpfner, M., Kiefer, M., Oelhaf, H., Orphal, J., Funke, B., Grabowski, U., Haanel, F., Linden, A., Wetzel, G., Woiwode, W., Bernath, P. F., Boone, C., Dutton, G. S., Elkins, J. W., Engel, A., Gille, J. C., Kolonjari, F., Sugita, T., Toon, G. C., and Walker, K. A.: MIPAS IMK/IAA CFC-11 (CCl<sub>3</sub>F) and CFC-12 (CCl<sub>2</sub>F<sub>2</sub>)  
445 measurements: accuracy, precision and long-term stability, *Atmos. Meas. Tech.*, 9, 3355–3389, <https://doi.org/10.5194/amt-9-3355-2016>, 2016.
- Eckert, E., von Clarmann, T., Laeng, A., Stiller, G. P., Funke, B., Glatthor, N., Grabowski, U., Kellmann, S., Kiefer, M., Linden, A., Babenhauserheide, A., Wetzel, G., Boone, C., Engel, A., Harrison, J. J., Sheese, P. E., Walker, K. A., and Bernath, P. F.: MIPAS IMK/IAA carbon tetrachloride (CCl<sub>4</sub>) retrieval and first comparison with other instruments, *Atmos. Meas. Tech.*, 10, 2727–2743,  
450 <https://doi.org/10.5194/amt-10-2727-2017>, 2017.



- Engel, A., Möbius, T., Bönisch, H., Schmidt, U., Heinz, R., Levin, I., Atlas, E., Aoki, S., Nakazawa, T., Sugawara, S., Moore, F., Hurst, D., Elkins, J., Schauffler, S., Andrews, A., and Boering, K.: Age of stratospheric air unchanged within uncertainties over the past 30 years, *Nature Geosci.*, 2, 28–31, <https://doi.org/10.1038/ngeo388>, 2009.
- Fischer, H., Birk, M., Blom, C., Carli, B., Carlotti, M., von Clarmann, T., Delbouille, L., Dudhia, A., Ehhalt, D., Endemann, M., Flaud, J. M., Gessner, R., Kleinert, A., Koopmann, R., Langen, J., López-Puertas, M., Mosner, P., Nett, H., Oelhaf, H., Perron, G., Remedios, J., Ridolfi, M., Stiller, G., and Zander, R.: MIPAS: an instrument for atmospheric and climate research, *Atmos. Chem. Phys.*, 8, 2151–2188, <https://doi.org/10.5194/acp-8-2151-2008>, 2008.
- Funke, B., López-Puertas, M., Gil-López, S., von Clarmann, T., Stiller, G. P., Fischer, H., and Kellmann, S.: Downward transport of upper atmospheric NO<sub>x</sub> into the polar stratosphere and lower mesosphere during the Antarctic 2003 and Arctic 2002/2003 winters, *J. Geophys. Res.*, 110, D24308, <https://doi.org/10.1029/2005JD006463>, 2005.
- Funke, B., García-Comas, M., López-Puertas, M., Glatthor, N., Stiller, G. P., von Clarmann, T., Semeniuk, K., and McConnell, J. C.: Enhancement of N<sub>2</sub>O during the October–November 2003 solar proton event, *Atmos. Chem. Phys.*, 8, 3805–3815, 2008.
- Funke, B., López-Puertas, M., García-Comas, M., Stiller, G. P., von Clarmann, T., Höpfner, M., Glatthor, N., Grabowski, U., Kellmann, S., and Linden, A.: Carbon monoxide distributions from the upper troposphere to the mesosphere inferred from 4.7 μm non-local thermal equilibrium emissions measured by MIPAS on Envisat, *Atmos. Chem. Phys.*, 9, 2387–2411, 2009.
- Funke, B., López-Puertas, M., Bermejo-Pantaleón, D., García-Comas, M., Stiller, G. P., von Clarmann, T., Kiefer, M., and Linden, A.: Evidence for dynamical coupling from the lower atmosphere to the thermosphere during a major stratospheric warming, *Geophys. Res. Lett.*, 37, L13803, <https://doi.org/10.1029/2010GL043619>, 2010.
- Funke, B., Baumgaertner, A., Calisto, M., Egorova, T., Jackman, C. H., Kieser, J., Krivolutsky, A., López-Puertas, M., Marsh, D. R., Reddmann, T., Rozanov, E., Salmi, S.-M., Sinnhuber, M., Stiller, G. P., Verronen, P. T., Versick, S., von Clarmann, T., Vyushkova, T. Y., Wieters, N., and Wissing, J. M.: Composition changes after the “Halloween” solar proton event: the High Energy Particle Precipitation in the Atmosphere (HEPPA) model versus MIPAS data intercomparison study, *Atmos. Chem. Phys.*, 11, 9089–9139, 2011.
- Funke, B., López-Puertas, M., Holt, L., Randall, C. E., Stiller, G. P., and von Clarmann, T.: Hemispheric distributions and interannual variability of NO<sub>y</sub> produced by energetic particle precipitation in 2002–2012, *J. Geophys. Res. Atmos.*, 119, 13,565–13,582, <https://doi.org/10.1002/2014JD022423>, 2014a.
- Funke, B., López-Puertas, M., Stiller, G. P., and von Clarmann, T.: Mesospheric and stratospheric NO<sub>y</sub> produced by energetic particle precipitation during 2002–2012, *J. Geophys. Res. Atmos.*, 119, 4429–4446, <https://doi.org/10.1002/2013JD021404>, 2014b.
- Funke, B., Ball, W., Bender, S., Gardini, A., Harvey, V. L., Lambert, A., López-Puertas, M., Marsh, D. R., Meraner, K., Nieder, H., Päivärinta, S.-M., Pérot, K., Randall, C. E., Reddmann, T., Rozanov, E., Schmidt, H., Seppälä, A., Sinnhuber, M., Sukhodolov, T., Stiller, G. P., Tsvetkova, N. D., Verronen, P. T., Versick, S., von Clarmann, T., Walker, K. A., and Yushkov, V.: HEPPA-II model-measurement intercomparison project: EPP indirect effects during the dynamically perturbed NH winter 2008–2009, *Atmos. Chem. Phys.*, 17, 3573–3604, <https://doi.org/10.5194/acp-17-3573-2017>, 2017.
- Garny, H., Birner, T., Bönisch, H., and Bunze, F.: The effects of mixing on age of air, *J. Geophys. Res. Atmos.*, 119, 7015–7034, <https://doi.org/10.1002/2013JD021417>, 2014.
- Haanel, F. J., Stiller, G. P., von Clarmann, T., Funke, B., Eckert, E., Glatthor, N., Grabowski, U., Kellmann, S., Kiefer, M., Linden, A., and Reddmann, T.: Reassessment of MIPAS age of air trends and variability, *Atmos. Chem. Phys.*, 15, 13 161–13 176, <https://doi.org/10.5194/acp-15-13161-2015>, 2015.
- Heggin, M. and Tegtmeier, S.: The SPARC Data Initiative, *SPARC Newsletter*, 36, 22–23, 2011.



- Hegglin, M. I. and Tegtmeier, S., eds.: The SPARC Data Initiative: Assessment of stratospheric trace gas and aerosol climatologies from satellite limb sounders, SPARC Report No. 8, WCRP-5/2017, SPARC, <https://doi.org/10.3929/ethz-a-010863911>, 2017.
- 490 Hegglin, M. I., Tegtmeier, S., Anderson, J., Froidevaux, L., Fuller, R., Funke, B., Jones, A., Lingenfelter, G., Lumpe, J., Pendlebury, D., Remsberg, E., Rozanov, A., Toohey, M., Urban, J., von Clarmann, T., Walker, K. A., Wang, R., and Weigel, K.: SPARC Data Initiative: Comparison of water vapor climatologies from international satellite limb sounders, *J. Geophys. Res. Atmos.*, 118, 11,824–11,846, <https://doi.org/10.1002/jgrd.50752>, 2013.
- 495 Kellmann, S., von Clarmann, T., Stiller, G. P., Eckert, E., Glatthor, N., Höpfner, M., Kiefer, M., Orphal, J., Funke, B., Grabowski, U., Linden, A., Dutton, G. S., and Elkins, J. W.: Global CFC-11 (CCl<sub>3</sub>F) and CFC-12 (CCl<sub>2</sub>F<sub>2</sub>) Measurements with the Michelson Interferometer for Passive Atmospheric Sounding (MIPAS): retrieval, climatologies and trends, *Atmos. Chem. Phys.*, 12, 11 857–11 875, <https://doi.org/10.5194/acp-12-11857-2012>, 2012.
- Lin, P. and Fu, Q.: Changes in various branches of the Brewer–Dobson circulation from an ensemble of chemistry climate models, *J. Geophys. Res.-Atmos.*, 118, 73–84, <https://doi.org/10.1029/2012JD018813>, 2013.
- 500 Madronich, S. and Flocke, S.: The role of solar radiation in atmospheric chemistry, in: *Handbook of Environmental Chemistry*, edited by Boule, P., pp. 1–26, Springer-Verlag, Heidelberg, 1998.
- Monge-Sanz, B. M., Chipperfield, M. P., Dee, D. P., Simmons, A. J., and Uppala, S. M.: Improvements in the stratospheric transport achieved by a chemistry transport model with ECMWF (re)analyses: identifying effects and remaining challenges, *Quart. J. Roy. Meteorol. Soc.*, 139, 654–673, <https://doi.org/10.1002/qj.1996>, 2012.
- 505 Pliening, J., von Clarmann, T., Stiller, G. P., Grabowski, U., Glatthor, N., Kellmann, S., Linden, A., Haenel, F., Kiefer, M., Höpfner, M., Laeng, A., and Lossow, S.: Methane and nitrous oxide retrievals from MIPAS-ENVISAT, *Atmos. Meas. Tech.*, 8, 4657–4670, <https://doi.org/10.5194/amt-8-4657-2015>, 2015.
- Pliening, J., Laeng, A., Lossow, S., von Clarmann, T., Stiller, G. P., Kellmann, S., Linden, A., Kiefer, M., Walker, K. A., Noël, S., Hervig, M., McHugh, M., Lambert, A., Urban, J., Elkins, J. W., and Murtagh, D.: Validation of revised methane and nitrous oxide profiles from MIPAS-ENVISAT, *Atmos. Meas. Tech.*, 9, 765–779, <https://doi.org/10.5194/amt-9-765-2016>, 2016.
- Ploeger, F., Abalos, M., Birner, T., Konopka, P., Legras, B., Müller, R., and Riese, M.: Quantifying the effects of mixing and residual circulation on trends of stratospheric mean age of air, *Geophys. Res. Lett.*, 42, 2047–2054, <https://doi.org/10.102/2014GL062927>, 2015a.
- Ploeger, F., Riese, M., Haenel, F., Konopka, P., Müller, R., and Stiller, G.: Variability of stratospheric mean age of air and of the local effects of residual circulation and eddy mixing, *J. Geophys. Res. Atmos.*, 120, 716–733, <https://doi.org/10.1002/2014JD022468>, 2015b.
- 515 Ploeger, F., Konopka, P., Walker, K., and Riese, M.: Quantifying pollution transport from the Asian monsoon anticyclone into the lower stratosphere, *Atmos. Chem. Phys.*, 17, 7055–7066, 2017.
- Plumb, R. A.: Stratospheric transport, *J. Meteorol. Soc. Jpn. Ser. II*, 80, 793–809, <https://doi.org/10.2151/jmsj.80.793>, 2002.
- Randel, W. J., Park, M., Emmons, L., Kinnison, D., Bernath, P., Walker, K. A., Boone, C., and Pumphrey, H.: Asian Monsoon Transport of Pollution to the Stratosphere, *Science*, 328, 611–613, <https://doi.org/10.1126/science.1182274>, 2010.
- 520 Ray, E. A., Moore, F. L., Elkins, J. W., Rosenlof, K. H., Laube, J. C., Röckmann, T., Marsh, D. R., and Andrews, A. E.: Quantification of the SF<sub>6</sub> lifetime based on mesospheric loss measured in the stratospheric polar vortex, *J. Geophys. Res. Atmos.*, 122, 4626–4638, <https://doi.org/10.1002/2016JD026198>, 2017.
- Reddmann, T., Ruhnke, R., and Kouker, W.: Three–dimensional model simulations of SF<sub>6</sub> with mesospheric chemistry, *J. Geophys. Res.*, 106, 14,525–14,537, <https://doi.org/10.1029/2000JD900700>, 2001.
- 525



- Sander, S. P., Friedl, R. R., Barker, J. R., Golden, D. M., Kurylo, M. J., Wine, P. H., Abbatt, J., Burkholder, J. B., Kolb, C. E., Moortgat, G. K., Huie, R. E., and Orkin, V. L.: Chemical kinetics and photochemical data for use in Atmospheric Studies, Evaluation Number 16 : supplement to Evaluation 15: update of key reactions, JPL Publication 09-31, Jet Propulsion Laboratory, National Aeronautics and Space Administration, Pasadena, CA, USA, 2010.
- 530 Smith, A. K., Garcia, R. R., Marsh, D. R., and Richter, J. H.: WACCM simulations of the mean circulation and trace species transport in the winter mesosphere, *J. Geophys. Res.*, 116, D20 115, <https://doi.org/10.1029/2011JD016083>, 2011.
- Stiller, G. P., Kiefer, M., Eckert, E., von Clarmann, T., Kellmann, S., García-Comas, M., Funke, B., Leblanc, T., Fetzer, E., Froidevaux, L., Gomez, M., Hall, E., Hurst, D., Jordan, A., Kämpfer, N., Lambert, A., McDermid, I. S., McGee, T., Miloshevich, L., Nedoluha, G., Read, W., Schneider, M., Schwartz, M., Straub, C., Toon, G., Twigg, L. W., Walker, K., and Whiteman, D. N.: Validation of MIPAS  
535 IMK/IAA temperature, water vapor, and ozone profiles with MOHAVE-2009 campaign measurements, *Atmos. Meas. Tech.*, 5, 289–320, <https://doi.org/10.5194/amt-5-289-2012>, 2012a.
- Stiller, G. P., von Clarmann, T., Haedel, F., Funke, B., Glatthor, N., Grabowski, U., Kellmann, S., Kiefer, M., Linden, A., Lossow, S., and López-Puertas, M.: Observed temporal evolution of global mean age of stratospheric air for the 2002 to 2010 period, *Atmos. Chem. Phys.*, 12, 3311–3331, <https://doi.org/10.5194/acp-12-3311-2012>, 2012b.
- 540 Stiller, G. P., Fierli, F., Ploeger, F., Cagnazzo, C., Funke, B., Haedel, F. J., Reddman, T., Riese, M., and von Clarmann, T.: Shift of subtropical transport barriers explains observed hemispheric asymmetry of decadal trends of age of air, *Atmos. Chem. Phys.*, 17, 11 177–11 192, <https://doi.org/10.5194/acp-17-11177-2017>, <https://doi.org/10.5194/acp-17-11177-2017>, 2017.
- Tegtmeier, S., Hegglin, M. I., Anderson, J., Bourassa, A., Brohede, S., Degenstein, D., Froidevaux, L., Fuller, R., Funke, B., Gille, J., Jones, A., Krüger, Y. K. K., Kyrölä, E., Lingenfelter, G., Lumpe, J., Nardi, B., Neu, J., Pendlebury, D., Remsberg, E., Rozanov, A., Smith, L.,  
545 Toohey, M., Urban, J., von Clarmann, T., Walker, K. A., and Wang, R. H. J.: SPARC Data Initiative: A comparison of ozone climatologies from international satellite limb sounders, *J. Geophys. Res. Atmos.*, 118, 12,229–12,247, <https://doi.org/10.1002/2013JD019877>, 2013.
- Tegtmeier, S., Hegglin, M. I., Anderson, J., Funke, B., Gille, J., Jones, A., Smith, L., von Clarmann, T., and Walker, K. A.: The SPARC Data Initiative: comparisons of CFC-11, CFC-12, HF and SF<sub>6</sub> climatologies from international satellite limb sounders, *Earth Syst. Sci. Data*, 8, 61–78, <https://doi.org/10.5194/essd-8-61-2016>, 2016.
- 550 Tung, K. K.: On the Two-Dimensional Transport of Stratospheric Trace Gases in Isentropic Coordinates, *J. Atmos. Sci.*, 39, 2330–2355, 1982.
- von Clarmann, T. and Grabowski, U.: Direct inversion of circulation and mixing from tracer measurements - Part 1: Method, *Atmos. Chem. Phys.*, 16, 14 563–14 584, <https://doi.org/10.5194/acp-16-14563-2016>, 2016.
- von Clarmann, T., Glatthor, N., Grabowski, U., Höpfner, M., Kellmann, S., Kiefer, M., Linden, A., Mengistu Tsidu, G., Milz, M., Steck, T., Stiller, G. P., Wang, D. Y., Fischer, H., Funke, B., Gil-López, S., and López-Puertas, M.: Retrieval of temperature and tangent altitude  
555 pointing from limb emission spectra recorded from space by the Michelson Interferometer for Passive Atmospheric Sounding (MIPAS), *J. Geophys. Res.*, 108, 4736, <https://doi.org/10.1029/2003JD003602>, 2003.
- von Clarmann, T., Höpfner, M., Kellmann, S., Linden, A., Chauhan, S., Funke, B., Grabowski, U., Glatthor, N., Kiefer, M., Schiederdecker, T., Stiller, G. P., and Versick, S.: Retrieval of temperature, H<sub>2</sub>O, O<sub>3</sub>, HNO<sub>3</sub>, CH<sub>4</sub>, N<sub>2</sub>O, ClONO<sub>2</sub> and ClO from MIPAS reduced resolution nominal mode limb emission measurements, *Atmos. Meas. Techn.*, 2, 159–175, <https://doi.org/10.5194/amt-2-159-2009>, 2009.
- 560 Waters, J. W., Froidevaux, L., Harwood, R. S., Jarnot, R. F., Pickett, H. M., Read, W. G., Siegel, P. H., Cofield, R. E., Filipiak, M. J., Flower, D. A., Holden, J. R., Lau, G. K., Livesey, N. J., Manney, G. L., Pumphrey, H. C., Santee, M. L., Wu, D. L., Cuddy, D. T., Lay, R. R., Loo, M. S., Perun, V. S., Schwartz, M. J., Stek, P. C., Thurstans, R. P., Boyles, M. A., Chandra, K. M., Chavez, M. C., Chen, G.-S., Chudasama, B. V., Dodge, R., Fuller, R. A., Girard, M. A., Jiang, J. H., Jiang, Y., Knosp, B. W., LaBelle, R. C., Lam, J. C., Lee, K. A., Miller, D.,



- 565 Oswald, J. E., Patel, N. C., Pukala, D. M., Quintero, O., Scaff, D. M., Van Snyder, W., Tope, M. C., Wagner, P. A., and Walch, M. J.: The Earth Observing System Microwave Limb Sounder (EOS MLS) on the Aura satellite, *IEEE Trans. Geosci. Remote Sens.*, 44, 1075–1092, <https://doi.org/10.1109/tgrs.2006.873771>, 2006.
- Waugh, D. W. and Hall, T. M.: Age of stratospheric air: theory, observations, and models, *Rev. Geophys.*, 40, 1010, <https://doi.org/10.1029/2000RG000101>, 2002.
- 570 Yu, P., Rosenlof, K. H., Liu, S., Telg, H., Thornberry, T. D., Rollins, A. W., Portmann, R. W., Bai, Z., Ray, E. A., Duan, Y., Pan, L. L., Toon, O. B., Bian, J., and Gao, R.-S.: Efficient transport of tropospheric aerosol into the stratosphere via the Asian summer monsoon anticyclone, *PNAS*, 114, 6972–6977, 2017.